Supporting Information for

Photothermal Coupling Electrolysis on Ni-W-B Toward Practical Overall Water Splitting

Weiju Hao,[a] Renbing Wu,*[a] Hongyuan Yang,[a] and Yanhui Guo*[a]

Dr. W. Hao, Prof. R. Wu, H. Yang, Prof. Y. Guo

[a]Department of Materials Science, Fudan University, Shanghai 200433, P. R. China

*E-mail: rbwu@fudan.edu.cn; gyh@fudan.edu.cn

Experimental Section

Materials

Nickel sulfate ($NiSO_4 \cdot 6H_2O$, AR), dimethyl ammonium borane (DMAB, AR), sodium sulfate (Na_2SO_4, AR), sodium succinate (AR), sodium tungstate ($Na_2WO_4 \cdot 2H_2O$, AR) were purchased from Sigma-Aldrich Chemical Reagent. Acetone (AR, 99.5%), ethanol (AR, 99.5%), nitric acid (HNO_3, AR), sulfuric acid (H_2SO_4, AR), Dipotassium phosphate (K_2HPO_4, AR), Potassium dihydrogen phosphate (KH_2PO_4, AR) and potassium hydroxide (KOH, AR) were bought from Aladdin. Carbon cloth (CC) about 0.1 mm in thickness was purchased from Shanghai Metal Company. Pt/C (10 wt% Pt), IrO_2 and Nafion (5 wt%) were purchased from Sigma-Aldrich Chemical Reagent. Water was ultrapure water which was purified through a Millipore system. All chemicals were used as received without further purification.

Preparation of Ni-W-B /CC electrode

In a typical preparation, Sodium sulfate (Na_2SO_4, 1.5 g) and sodium succinate (2.5 g) were dissolved in 100 mL water and stirred at 450 rmp min^{-1}. After 30 min, the Nickel sulfate hexahydrate ($NiSO_4 \cdot 6H_2O$, 2.5 g) was added and the solution system became a stability of

metal complexes. Then the dimethyl ammonium borane (DMAB, 0.72 g) and sodium tungstate dihydrate ($Na_2WO_4 \cdot 2H_2O$, 0.157 g) were dispersed in the system and dissolved completely. 100 mL of the solution was divided into 5 equal and filled into beaker for later use. A piece of carbon cloth (CC, 1 cm × 0.5 cm) was treated with dilute nitric acid at 90 °C for 12 h and then cleaned by water and ethanol. The cleaned CC was immersed into the pre-prepared solution. The electroless plating of CC was maintained at room temperature (25 °C) for 30 min, 60 min, 90 min, 120 min and 150 min. At last, the roughness of the surface of Ni-W-B/CC was prepared (5.6 mg cm^{-2}) for the best performance (Fig. S1, Supporting information).

Characterizations

X-ray diffractometer (XRD) was acquired on a Rigaku D/MAX 2550 with Cu Kα radiation. Scanning electron microscopic (SEM) measurements were performed on a HitachiS-4800 field at an accelerating voltage of 20 kV. Transmission electron microscopy (TEM, JEOL Ltd., JEM-2100F) was employed to analyze the microstructure of a single Ni-W-B catalyst. X-ray photoelectron spectrometer (XPS) data were collected on an ESCALABMK II using Mg as the exciting source. The binding energy was calibrated by means of the C 1s peak energy of 284.6 eV. Inductively coupled plasma atomic emission spectroscopy (ICP-AES) analysis was performed on Model ARCOS FHS12 (SPECTRO Analytical Instruments Inc, Germany). Light (the intensity of light was about 0.75 W cm^{-2}) was supplied by a Xenon lamp (LSP-X500 Arc lamp), the intensity of light was detected by the Solar Power Meter (SM206-SOLAR).

PTE experimental work process

All photothermal effect (PTE) measurements were performed in a three electrode mode with a photothermal catalyst (Ni-W-B/CC), a carbon rod and an Ag/AgCl as the working, counter and reference electrode within a transparent glass beaker. 1.0 M KOH (0.5 M phosphate

buffer saline (PBS) and 0.5 M H_2SO_4) aqueous solution was used as the electrolyte. All Ni-W-B/CC electrodes were illuminated from the front side using a Xenon lamp (LSP-X500 Arc lamp) to simulate the solar spectrum. The light intensity was calibrated to 0.75 W cm^{-2} by a convex lens (Conventional type, Diameter =10 cm) during the electrochemical test.

Electrochemical Measurements

Linear-sweep voltammetry (LSV) curves were recorded from a CHI760E electrochemcial workstation (Chenhua, Shanghai). A three-electrode cell system was employed using a Ni-W-B/CC (CC: 0.5 cm^2) as working electrode, a carbon rod as the counter-electrode and saturated calomel electrode as reference electrode. In all measurements, the saturated calomel electrode reference electrode was calibrated with respect to the RHE. LSV measurements were conducted in 1.0 M KOH, 0.5 M PBS or 0.5 M H_2SO_4 at a scan rate of 5 mV S^{-1} without *iR*-correction. All potentials reported were calibrated to the RHE. In 1.0 M KOH (0.5 M PBS or 0.5 M H_2SO_4), *E* (RHE) = *E* (SCE) + 0.245 V + 0.0596 pH, where *E* was the potential of the electrode[1]. For comparison, the working electrodes using Pt-C/CC and IrO_2/CC were also investigated. In the preparation of Pt/C electrode, 5 mg Pt-C, 30 μL nafion solution and 970 μL ethanol were mixed and ultrasounding for 30 min. An aliquot of 10 μL was pipetted onto the CC (0.5 cm^2) for several times to reach a catalyst loading about 5.6 mg cm^{-2}. IrO_2/CC was prepared using the same method and the results of overpotential were also not *iR*-corrected. The stability of a catalyst was carried by chronopotentionmetry at a constant potential or current density, the time was 20 h at the current density.

Electrochemical Surface Area (ECSA) Determination

The double-layer capacitance (C_{dl}), which is in proportion to ECSA,[2] was obtained by deriving from the cyclic voltammery (CV) curves versus the scan rates. The potential was swept between 0.05 and 0.17 V versus RHE at five different scan rates (5, 25, 45, 65 and 85 mV s^{-1}) for HER. The potential was swept between 0.70 and 0.86 V versus RHE at eight

different scan rates (5, 25, 45, 65 and 85 mV s^{-1}) for OER. The measured C_{dl} are plotted as a function of scan rate. The C_{dl} of HER for Ni-W-B/CC and Ni-W-B/CC (PTE) are determined as 115.1 mF cm^{-2}, and 135.2 mF cm^{-2}, respectively (Fig. S13, Supporting information). The C_{dl} of OER for Ni-W-B/CC and Ni-W-B/CC (PTE) were determined as 39.1 mF cm^{-2} and 41.1 mF cm^{-2}, respectively (Fig. S14, Supporting information).

The remarkably improved activity at high temperature during the water spliting can be analyzed as following:[3]

$$H_2O \rightarrow O_2 + 4H^+ + 4e^- \quad (1)$$

$$\Delta G = \Delta H - T\Delta S \quad (2)$$

$$E_{rev} = -\frac{\Delta G}{2F} \quad (3)$$

$$E_{rev} = 1.23 - 0.9 \times 10^{-3}(T - 298) \quad (4)$$

$$E_{Nernst} = E_{rev} + \frac{RT}{4F}\ln\left[(H^+)^4 P_{O_2}\right] \quad (5)$$

$$\Delta E = (0.9 \times 10^{-3} + 1.99 \times 10^{-4}\ PH)\Delta T \quad (6)$$

Eq (1): The thermodynamics of the water oxidation reaction is altered by the elevating temperature;

Eq (2): The Gibbs free energy (△G) is mathematically expressed, where △H is the enthalpy and △S is the entropy of the reaction;

Eq (3): The reversible potential (E_{rev}) based on the Gibbs free energy is given by, where F is the Faraday constant.

Eq (4): Considering that Gibbs free energy is temperature dependent, an empirical expression of the reversible potential for water oxidation has been reported to model this behavior.

Eq (5): Influenced by the concentration of the reactants and products, the reversible potential is evolved to give the Nernst potential (ENernst);

Eq (6): the change of Nernst potential resulting from the elevated temperature of electrolyte system.

In this work, substituting pH 14 in eq (6) results in a slope of -3.686 mV $^{o}C^{-1}$ which was the temperature coefficient of the water oxidation reaction attributed to thermodynamics.

The experimental temperature coefficient (-3.790 mV $^{o}C^{-1}$, Fig. 3e and 3f) of the onset potential of the Ni-W-B/CC was substantially similar to the equation (-3.686 mV $^{o}C^{-1}$). In fact, the temperature of the electrolyte only increased by 0.9 ^{o}C (Fig. S9, Supporting information), corresponding to an overpotential reduction of 3.411 mV for Ni-W-B/CC electrode operated at the elevated temperature of electrolyte. However, the overpotential was decreased by 39 mV at the current density of 100 mA cm^{-2} under PTE deduced from the thermodynamic change of the water oxidation reaction.

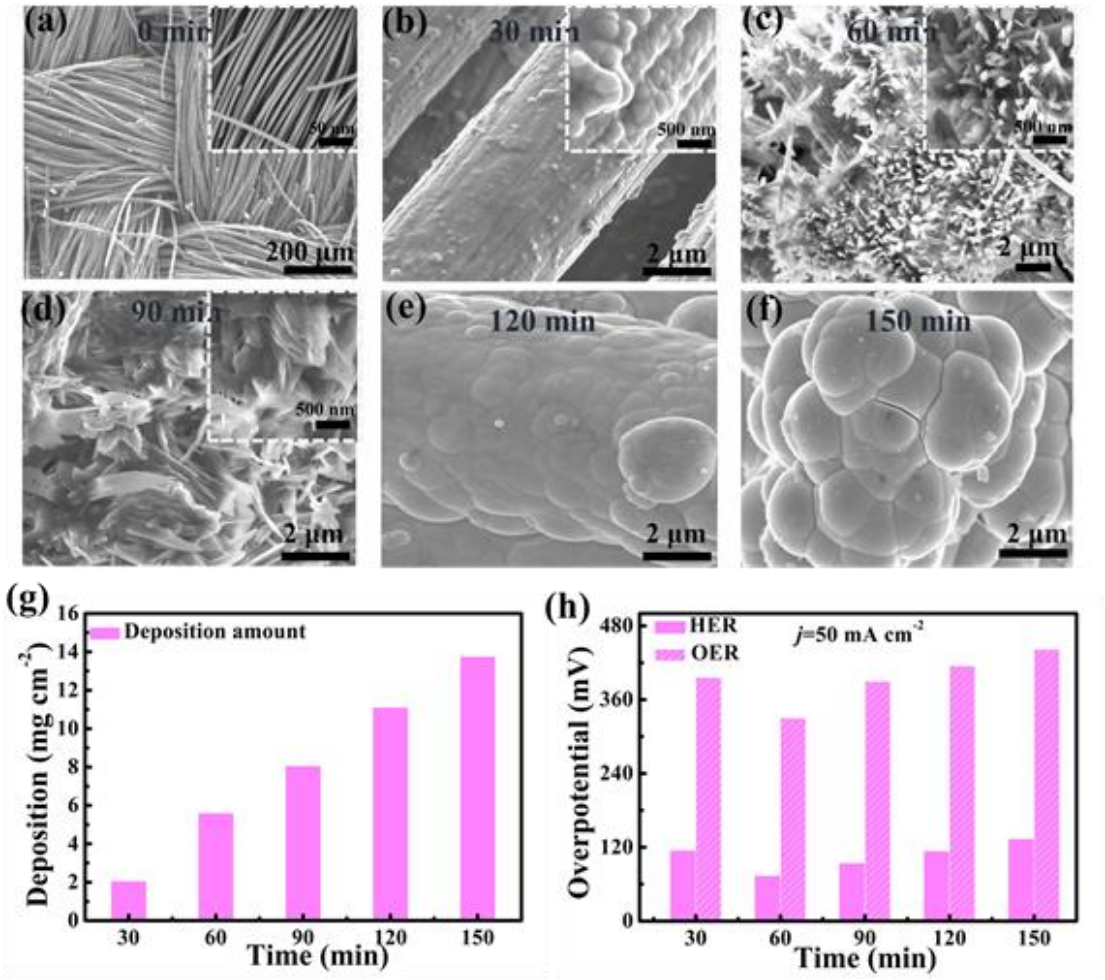

Figure S1. FESEM images of Ni-W-B/CC electrode during its formation process at 25 °C (a-f), the amount of catalyst deposited on the CC substrate (g) and the overpotentials of HER and OER for the Ni-W-B/CC electrode at different time.

Table S1. ICP-AES analysis on the Ni-W-B/CC electrode.

Catalysts	**ICP-AES (wt%)**			**Atomic ratio**
	Ni	**W**	**B**	**Ni:W:B**
Ni-W-B	84.81	6.38	2.38	6.5:0.16:1
Post-HER	82.42	6.33	2.10	7.2:0.18:1
Post-OER	83.11	6.14	1.98	7.7:0.18:1

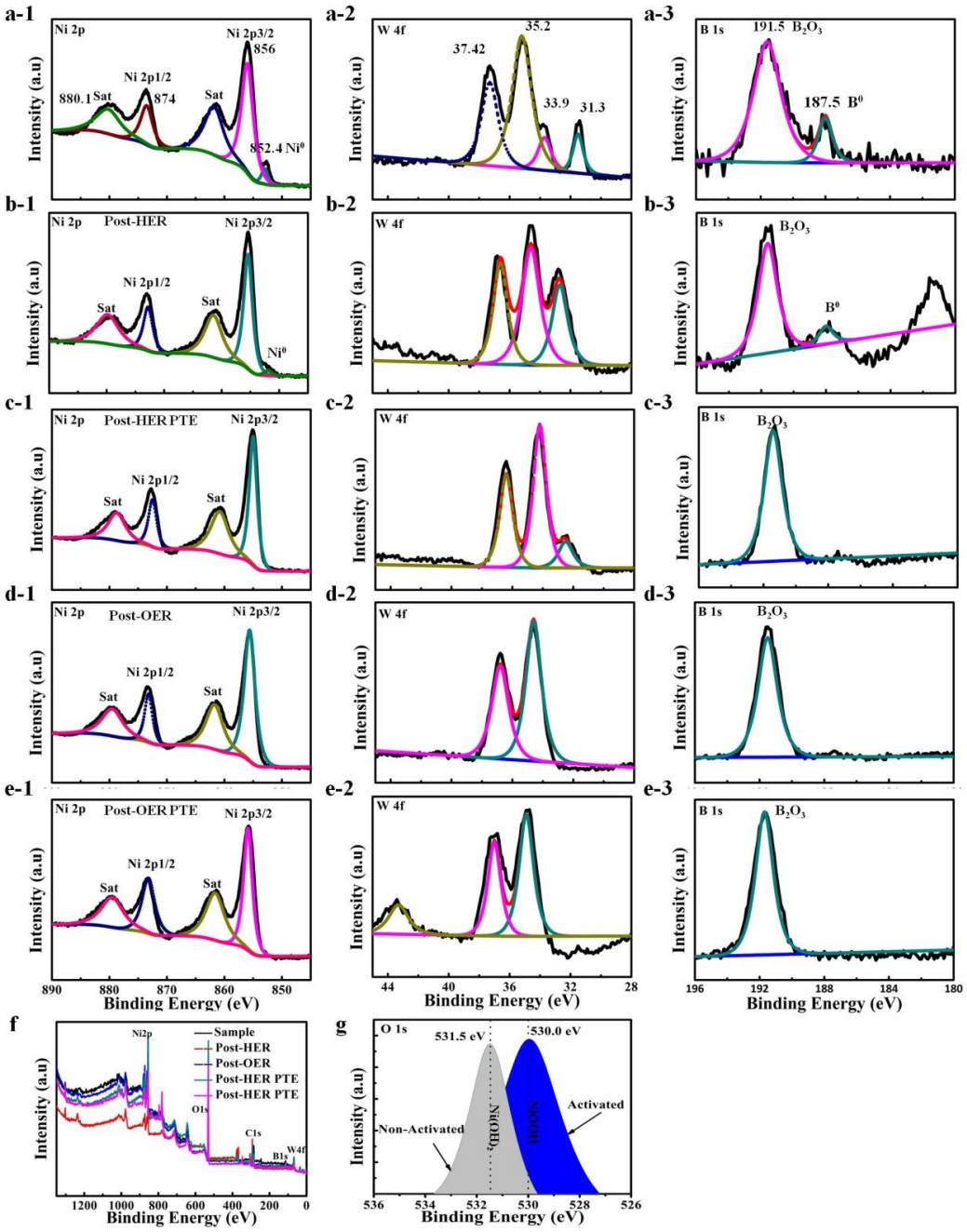

Figure S2. (a-1, a-2 and a-3) Ni 2p, W 4f and B 1s core-level XPS spectra of Ni-W-B/CC, respectively. (b-1, b-2 and b-3) XPS spectra for the post-HER of Ni-W-B/CC in the Ni 2p, W 4f and B 1s. (c-1, c-2 and c-3) post-HER with PTE of Ni-W-B/CC in the Ni 2p, W 4f and B 1s. (d-1, d-2, d-3) XPS spectra for the post-OER Ni-W-B/CC with PTE. (e-1, e-2,e-3) XPS spectra for the post-OER of Ni-W-B/CC with PTE. (f) XPS survey spectrum of Sample, Post-HER, Post-OER and Post-HER (PTE), Post-OER (PTE) of Ni-W-B/CC. (g) O 1s high-resolution spectra of Ni-W-B/CC before and post-OER with PTE.

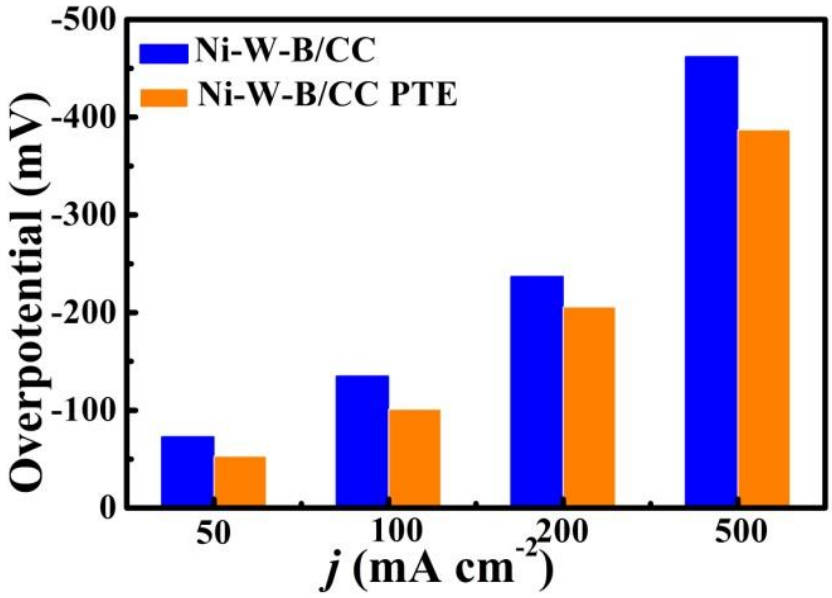

Figure S3. Overpotentials of Ni-W-B/CC and PTE-promoted Ni-W-B/CC for HER at current densities of 50, 100, 200 and 500 mA cm^{-2}.

Table S2. Comparison of the HER performances of Ni-W-B/CC with other state-of-the-art electrocatalysts in 1.0 M KOH.

Catalysts	***j* (mA cm^{-2})**	**η (HER: mV)**	**Reference**
Ni-W-B/CC	**50/100**	**73/136**	**This work**
Ni-W-B/CC(PTE)	**50/100**	**53/101**	
CoP NWs/CC	100	180	[4]
$Ni_{1-x}CoxSe_2$/NF	10	85	[5]
Se-(NiCo)Sx/(OH)x/NF	10	103	[6]
Co-Ni_3N	40	220	[7]
FeB_2/NF	10	61	[8]
CoPS/NF	10	48	[9]
Ni_2P/Fe_2P-NF	10	121	[10]
Co-W-B/NF	10	90	[11]
FeS_2/CoS_2	10	78	[12]

NiP/NF	10	42	[13]
Fe-Ni@NC-CNTs	145	202	[14]
MoP/NF	10	110	[15]
$CoP/Ni_5P_4/CoP/NF$	10	71	[16]
FeCoNi-HNTAs/NF	10	58	[17]
Ni_2P-NiP_2/NF	10	59.7	[18]
NiFe NTAs-NF	10	181	[19]
NiFeSP/NF	10	91	[20]

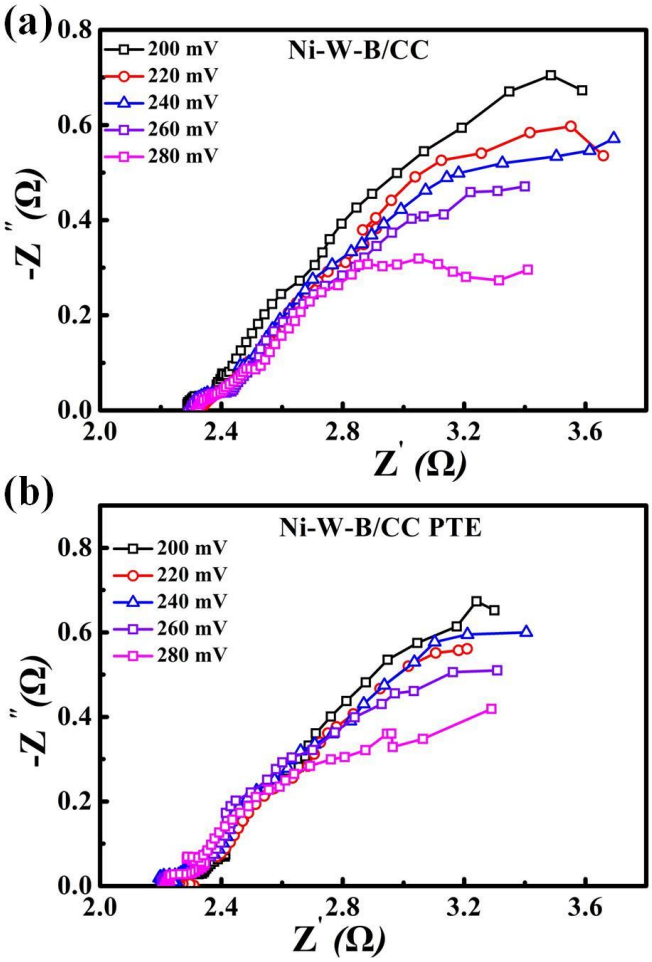

Figure S4. Electrochemical impedance spectroscopy of Ni-W-B/CC (a) and Ni-W-B/CC with PTE (b) for HER.

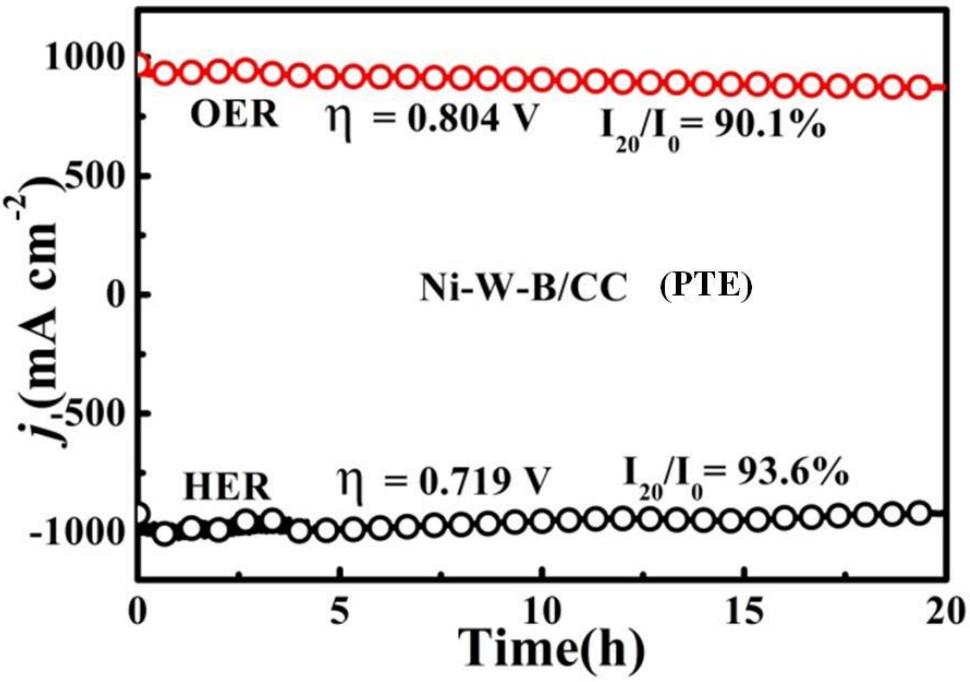

Figure S5. Long-term stability test of Ni-W-B/CC at current density of 1000 mA cm^{-2} for HER and OER in 1 M KOH over 20 h with PTE**.**

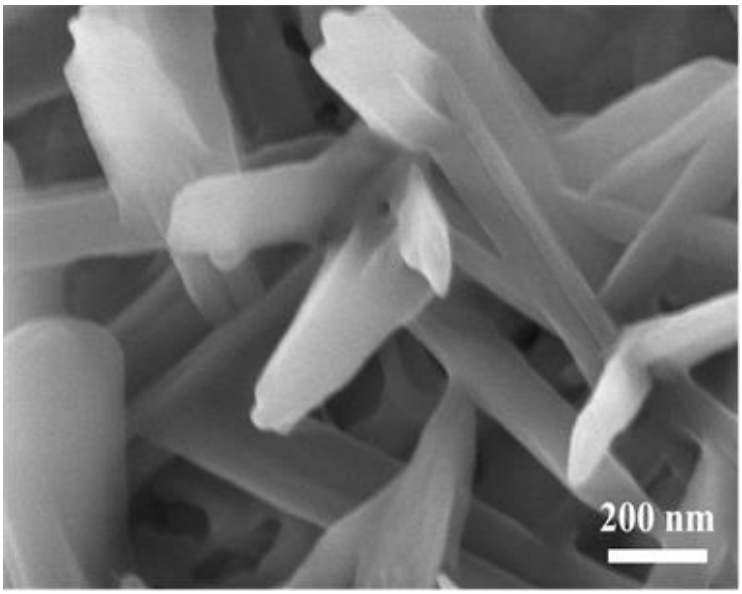

Figure S6. SEM image of post-HER Ni-W-B/CC (PTE) for 20 h.

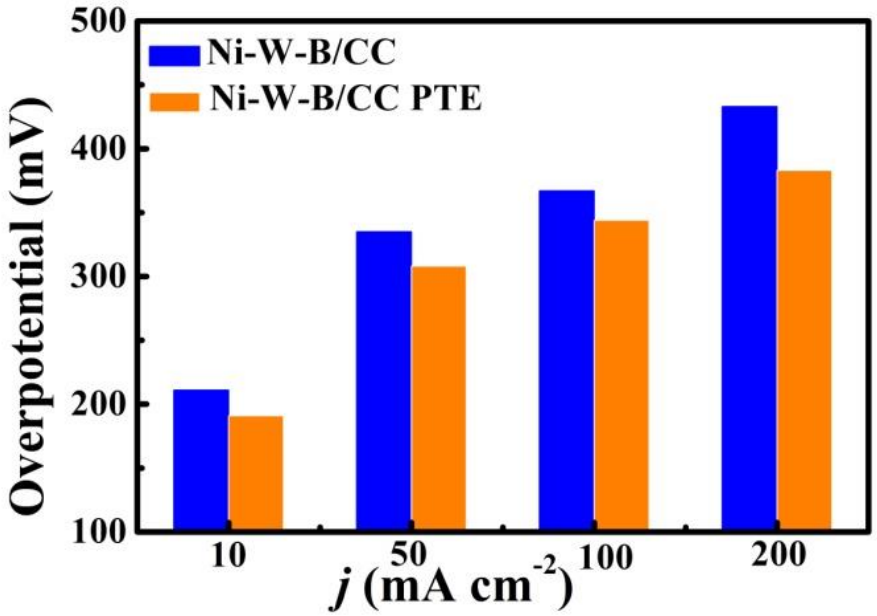

Figure S7. Required overpotentials at a current density of 10, 50, 100 and 200 mA cm^{-2} for OER.

Table S3. Comparison of OER performance in 1.0 M KOH for Ni-W-B/CC with other non-noble-metal electrocatalysts.

Catalyst	***j*** **(mA cm^{-2})**	**η(OER.mV)**	**Reference**
Ni-W-B/CC	**10/50/100**	**211/332/367**	**This work**
Ni-W-B/CC(PTE)	**10/50/100**	**191/302/344**	
Ni(BDC) @NF	10	265	[21]
Fe-Doped Ni_2P	10	230	[22]
Co-MoS_2/NF	10	260	[23]
$CoNiO_2$	10	210	[24]
Fe-Co-$NiSe_2$	10	251	[25]
WO_2 HN/NF	10	300	[26]
Co_9S_8/GC	10	302	[27]

$Co_{5.47}$N-NP@N-PC	10	248	[28]
Fe-doped $NiCr_2O_4$/NF	10	228	[29]
$Fe(TCNQ)_2$ nanowire	10	340	[30]
Co-M-P-NS	10	209	[31]
MnO_2-CoP_3	10	280	[32]
$F_{0.25}C_1$CH/NF	10	228	[33]
Fe-CoP/Ti mesh	10	230	[34]
NixB/NF	10	280	[1]
NiCoP/NF	10	280	[35]
Ni_2P/NF	10	277	[36]
Ni/Mo_2C-PC	10	368	[37]

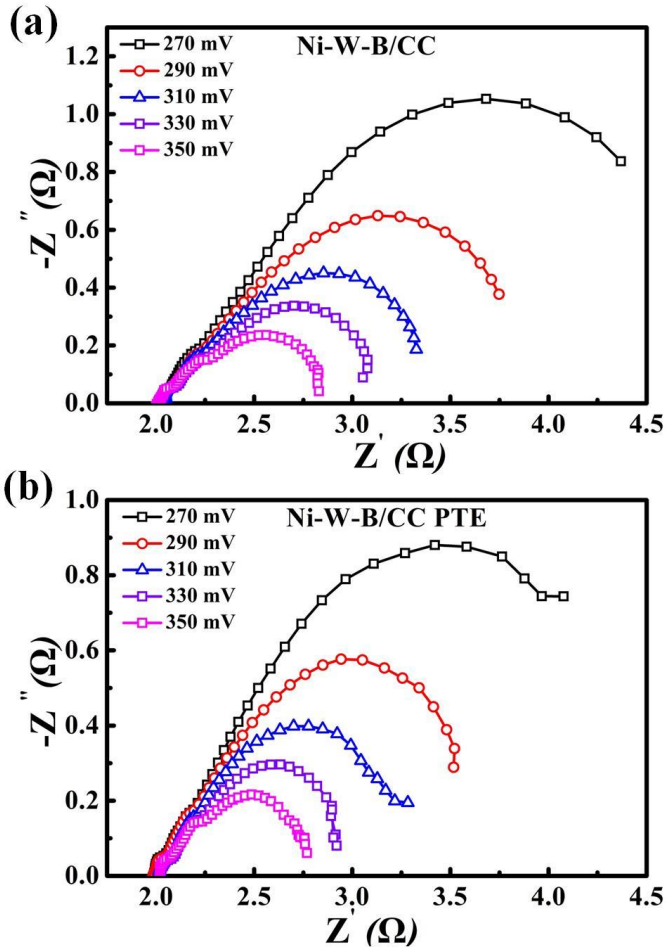

Figure S8. Electrochemical impedance spectroscopy of Ni-W-B/CC (a) and Ni-W-B/CC with PTE(b) for OER.

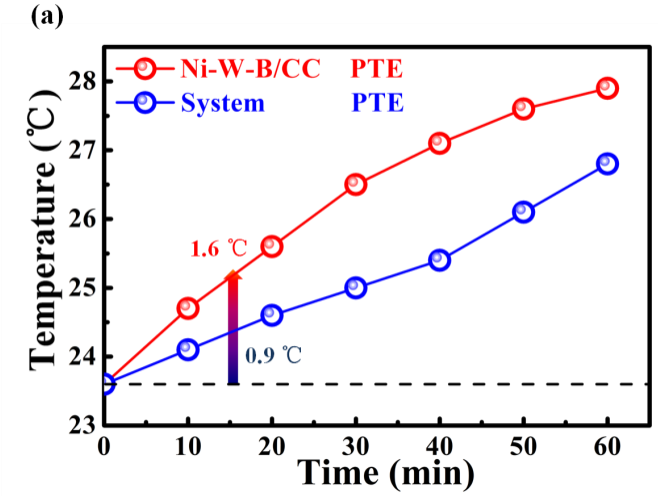

(b)

Timie (min) PTE	Ni-W-B/CC (℃)	System (℃)
0	23.6	23.6
10	24.7	24.1
20	25.6	24.6
30	26.5	25
40	27.1	25.4
50	27.6	26.1
60	27.9	26.8

Figure S9. (a) and (b) The temperature changes of system, electrolyte close to the Ni-W-B/CC under PTE.

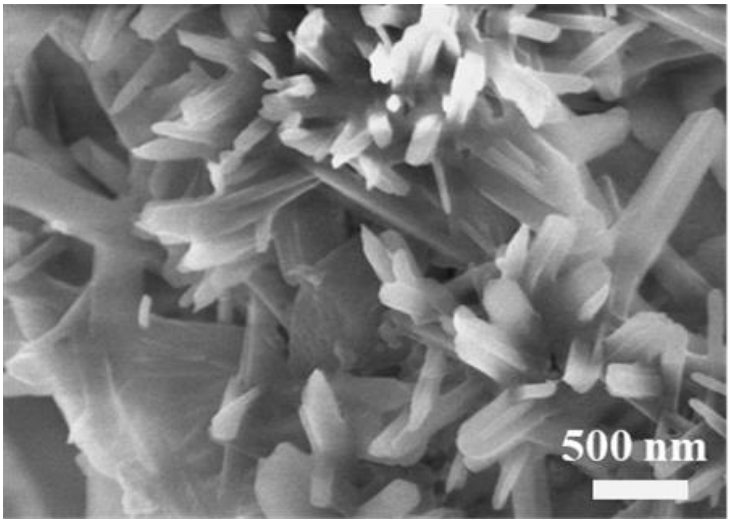

Figure S10. SEM image of post-OER (PTE) Ni-W-B/CC for 20 h.

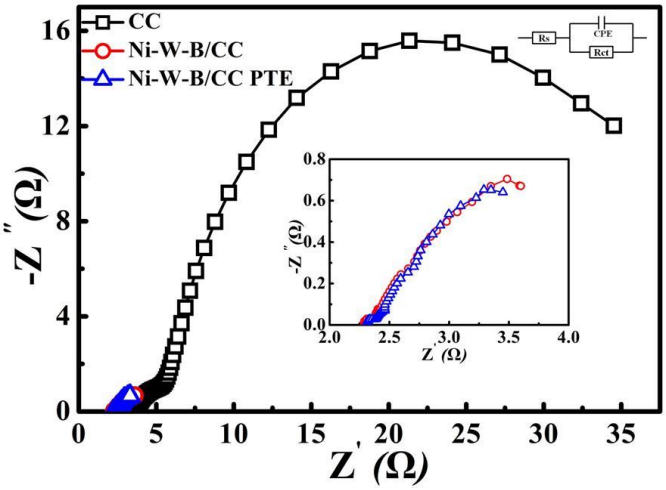

Figure S11. Nyquist plots of CC and Ni-W-B/CC measured at overpotential of 200 mV for HER.

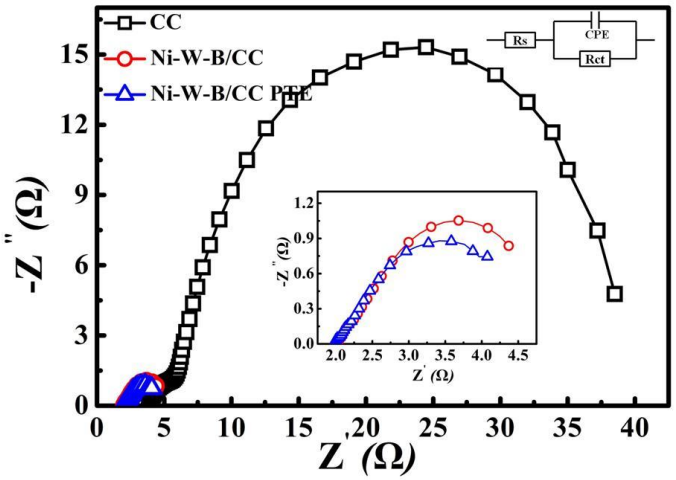

Figure S12. Nyquist plots of CC and Ni-W-B/CC measured at overpotential of 270 mV for OER.

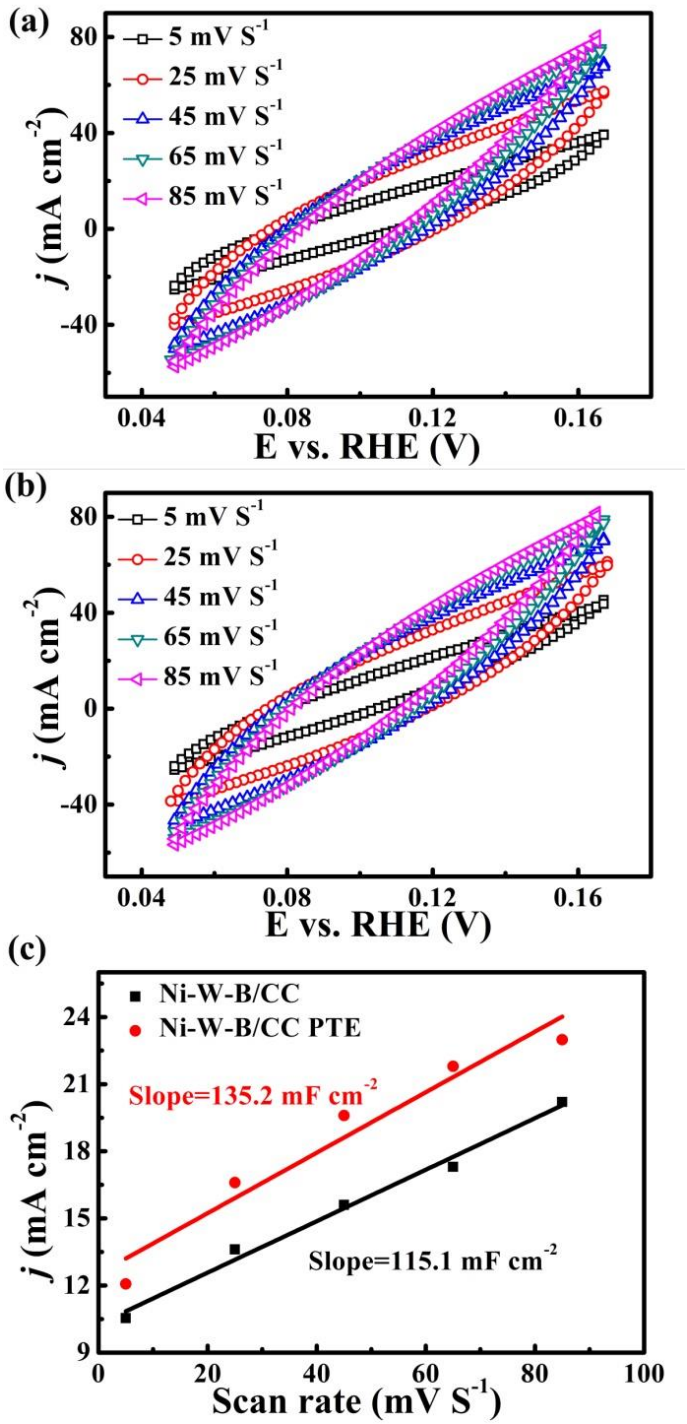

Figure S13. Electrochemical capacitance measurements to determine the surface area of the obtained electrodes in 1 M KOH for HER. The capacitive current density on (a) Ni-W-B/CC, (b) Ni-W-B/CC PTE from double layer charging can be measured from cyclic voltammograms in a potential range where no Faradic reaction occur. (c) The measured capacitive current plotted as a function of scan rateat 0.10 V vs. RHE.

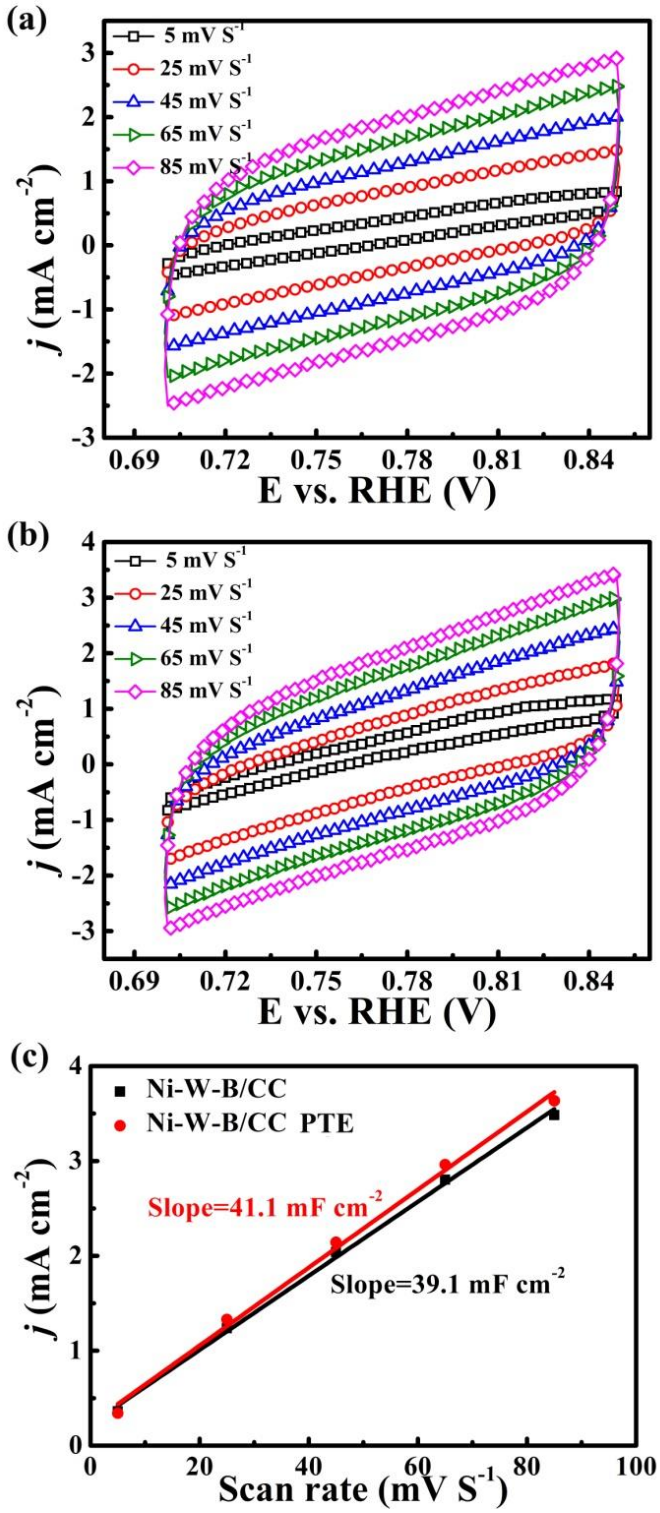

Figure S14. Electrochemical capacitance measurements to determine the surface area of the obtained electrodes in 1 M KOH for OER. The capacitive current density on a) Ni-W-B/CC, b)Ni-W-B/CC PTE from double layer charging can be measured from cyclic voltammo grams at scan rates from 5 to 85 mV s^{-1} in a potential range where no Faradic reaction occur. c) The measured capacitive current plotted as a function of scan rateat 0.78 V vs.RHE.

Table S4. Comparison of overall water splitting performance in 1.0 M KOH for Ni-W-B/CC with other non-noble-metal electrocatalysts.

Catalyst	***j*** **(mA cm^{-2})**	***Voltages*** **(V)**	**Reference**
Ni-W-B/CC	**25**	**1.631**	**This work**
	100	**1.794**	
Ni-W-B/CC (PTE)	**25**	**1.524**	
	100	**1.678**	
NC-NiCu-NiCuN	10	1.56	[38]
NiFeSP/NF	10	1.58	[20]
N-Ni_3S_2/NF	10	1.48	[39]
Fe,Co-$NiSe_2$/CF	10	1.52	[40]
Ni-Mo-O/CC	10	1.54	[41]
$CoSn_2$/NF	10	1.55	[42]
2D LMH(M □□Ni, Fe, Co, NiFe, and NiCo)	10	1.55	[43]
NiFeSP/NF	10	1.58	[44]
CoOx@CN	10	1.55	[45]
CoMnCH/NF	10	1.68	[46]
CoP/NCNHP	10	1.64	[47]
Pt-CoS_2/CC	10	1.55	[48]
G-Ni_4Fe/GF	10	1.58	[49]
Mo_2C-PC/NF	10	1.66	[50]

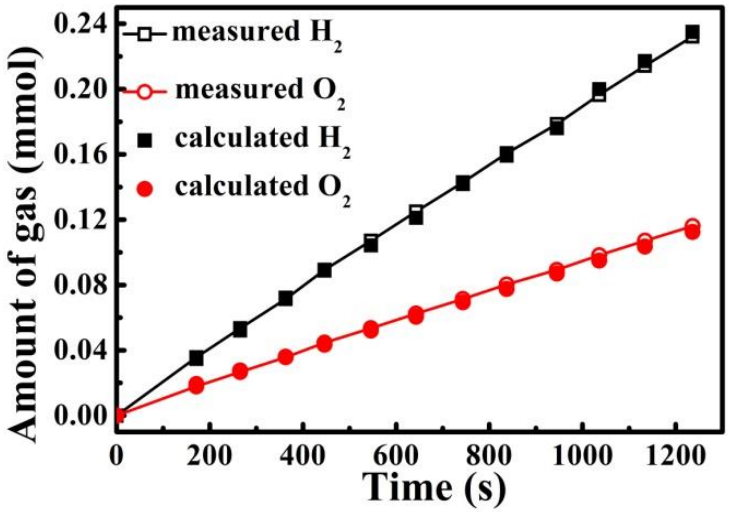

Figure S15. Amount of gas theoretically calculated and experimentally measured versus time for Ni-W-B/CC||Ni-W-B/CC with PTE.

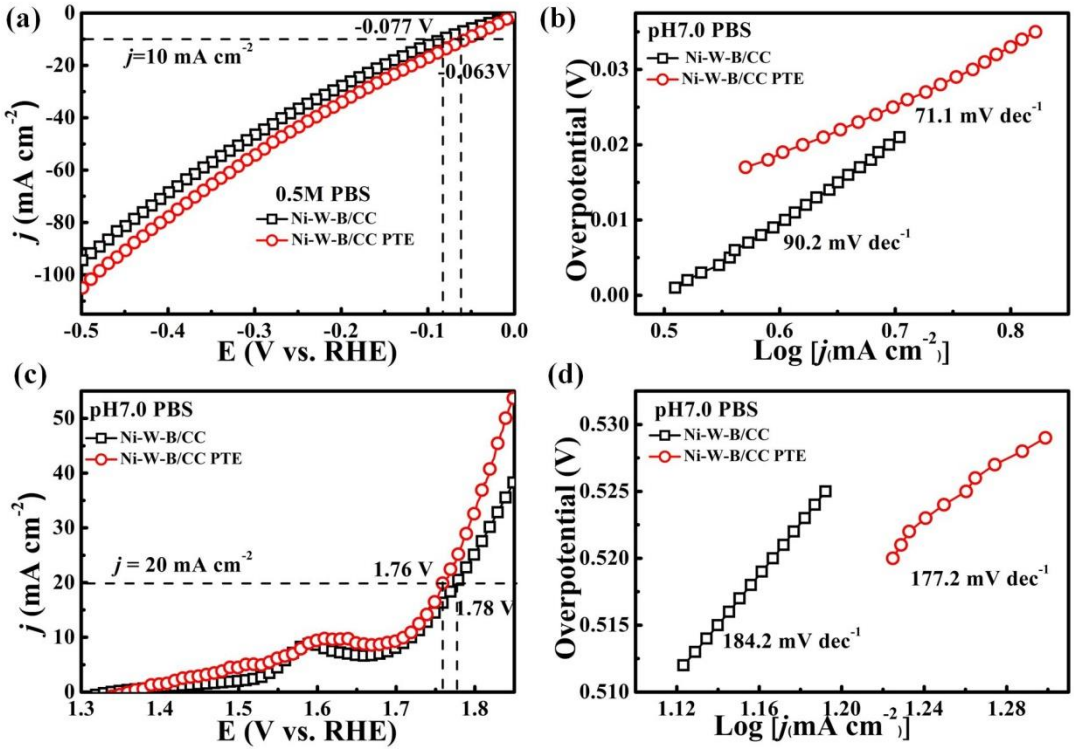

Figure S16. (a) HER polarization curves and (b) Tafel slope of Ni-W-B/CC electrode and Ni-W-B/CC electrode with PTE in 0.5 M PBS (pH = 7.0). (c) OER polarization curves and (d) tafel slope of Ni-W-B/CC electrode and Ni-W-B/CC electrode with PTE in 0.5 M PBS (pH = 7.0).

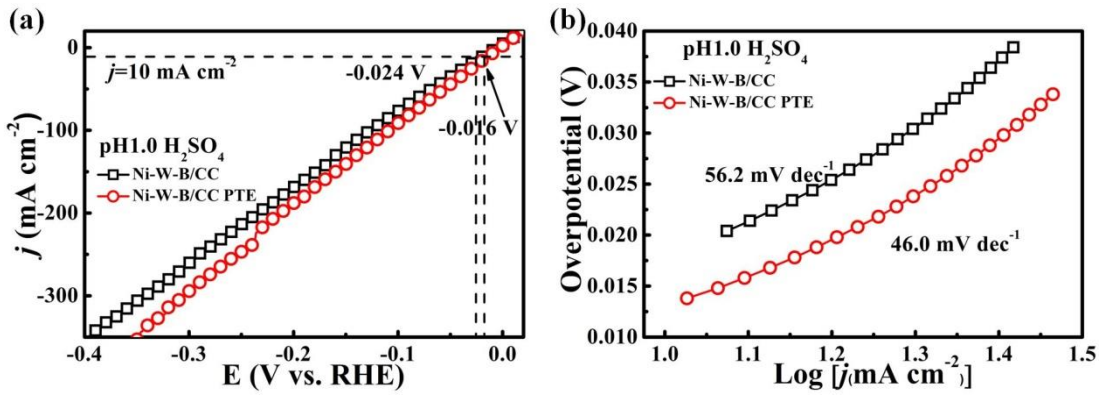

Figure S17. (a) HER polarization curves and (b) tafel slope of Ni-W-B/CC electrode and Ni-W-B/CC electrode with PTE in 0.5 M H_2SO_4 (pH = 1.0).

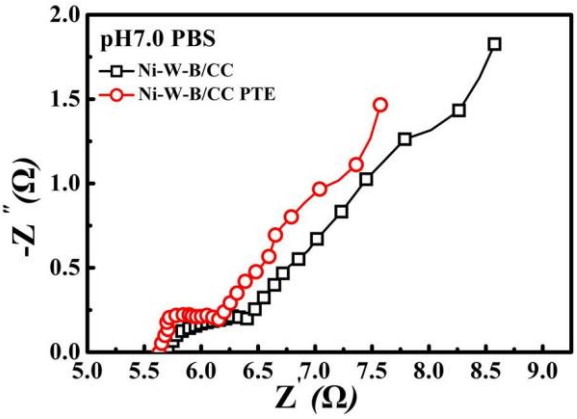

Figure S18. Nyquist plots of Ni-W-B/CC and Ni-W-B/CC (PTE) measured at overpotential of 150 mV for HER in 0.5 M PBS (pH 7.0).

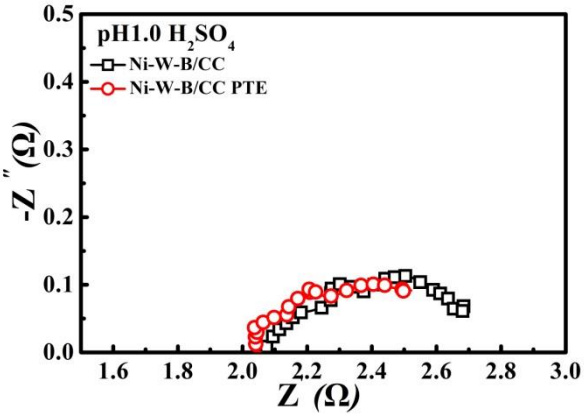

Figure S19. Nyquist plots of Ni-W-B/CC and Ni-W-B/CC (PTE) measured at overpotential of 150 mV for HER in 0.5 M H_2SO_4 (pH 1.0).

References

1. J. Masa, I. Sinev, H. Mistry, E. Ventosa, M. de la Mata, J. Arbiol, M. Muhler, B. R. Cueny and W. Schuhmann, *Adv. Energy Mater.*, 2017, **7**, 1700381.
2. L.A. Stern, F. Song and X.L. Hu, *Energy Environ. Sci*, 2015, **8**, 2347.
3. B.B Zhang, M. Cheng, L.Z. Fan and L. Sun, *Faraday Discuss.*, 2017, **198**, 169.
4. K. Xu, H. Cheng, H. Lv, J. Wang, L. Liu, S. Liu, X. Wu, W. Chu, C. Wu and Y. Xie, *Adv Mater*, 2018, **30**. 1705516.
5. B. Liu, Y. F. Zhao, H. Q. Peng, Z. Y. Zhang, C. K. Sit, M. F. Yuen, T. R. Zhang, C. S. Lee and W. J. Zhang, *Adv. Mater.*, 2017, **29**. 1606521.
6. C. Hu, L. Zhang, Z. J. Zhao, A. Li, X. Chang and J. Gong, *Adv. Mater.*, 2018, **30**, e1705538.
7. C. Zhu, A. L. Wang, W. Xiao, D. Chao, X. Zhang, N. H. Tiep, S. Chen, J. Kang, X. Wang, J. Ding, J. Wang, H. Zhang and H. J. Fan, *Adv. Mater.*, 2018, **30**, e1705516.
8. H. Li, P. Wen, Q. Li, C. Dun, J. Xing, C. Lu, S. Adhikari, L. Jiang, D. L. Carroll and S. M. Geyer, *Adv. Energy Mater.*, 2017, **7**, 1700513.
9. M. Cabán-Acevedo, M. L. Stone, J. R. Schmidt, J. G. Thomas, Q. Ding, H.-C. Chang, M.-L. Tsai, J.-H. He and S. Jin, *Nat. Mater.*, 2015, **14**, 1245.
10. Y. Ge, P. Dong, S. R. Craig, P. M. Ajayan, M. Ye and J. Shen, *Adv. Energy Mater.*, 2018, 1800484.
11. G.X. Cao, N. Xu, Z.J. Chen, Q. Kang, H.B. Dai and P. Wang, *ChemistrySelect*, 2017, **2**, 6187-6193.
12. Y.X. Li, L. An, M. Lu, K. Sun, Y.Q. Zhao, D.Q. Gao, F.Y. Cheng, and P. Xi, *Small*, 2018, **14**, 1801070.
13. P. Menezes, C. Panda, S. Loos, F. B. Bruns, C. Walter, M. Schwarze, X. Deng, H. Dau and M. Driess, *Energy Environ. Sci.*, 2018, **11**, 1287-1298.
14. X. Zhao, P. Pachfule, S. Li, J. R. J. Simke, J. Schmidt and A. Thomas, *Angew. Chem. Int. Ed.*, 2018, **57**, 8921-8926.
15. Y. Jiang, Y. Lu, J. Lin, X. Wang and Z. Shen, *Small Methods*, 2018, **2**, 1700369.
16. I. K. Mishra, J.Y. Sun, F. Qin, K. Dahal, and J.M. Bao, *Energy Environ. Sci*, 2018, DOI: 10.1039/c8ee01270a.
17. H. Li, S. Chen, Y. Zhang, Q. Zhang, X. Jia, L. Gu, X. Sun, L. Song and X. Wang, *Nat Commun*, 2018, **9**, 2452.
18. T. Liu, A. Li, C. Wang, W. Zhou, S. Liu and L. Guo, *Adv. Mater.*, 2018, e1803590.
19. L. Xu, J.H. Chen, X.Z. Fu, R. Sun, and C.P. Wong, *ACS Appl. Energy Mater.* , 2018, **1**, 1210-1217.

20. Y.M. Xin, L.Y. Gan, and Z.H.Zhang, *ACS Nano* 2018, **11**, 10303-10312.
21. H. Sun, Y. Lian, C. Yang, L. Xiong, P. Qi, Q. Mu, X. Zhao, J. Guo, Z. Deng and Y. Peng, *Energy Environ. Sci.*, 2018, **10**, 2363-2371.
22. Y. Li, H. Zhang, M. Jiang, Q. Zhang, P. He and X. Sun, *Adv. Funct. Mater.*, 2017, **27**, 1702513.
23. Q.Z Xiong, P.F. Liu, L.R. Zheng, G.Z Wang, *Adv. Mater.*, 2018, **30**, 1801450.
24. Y.Z. Jin, Z. Li, J.Q. Wang, R. Li, Z.Q. Li, H. Liu, J. Mao, *Adv. Energy Mater.*, 2018, **8**, 1703469.
25. Y.Q Sun, Z.X. Wei, H.L. Li, T. Zhang, X.Y. Li, W.P. Cai, and J.M. Ma, and Y. Li, *Adv. Mater.*, 2018, 1802121.
26. C. Shu, S. Kang, Y. Jin, X. Yue and P. K. Shen, *J. Mater. Chem. A*, 2017, **5**, 9655-9660.
27. Z. Chen, R. Wu, M. Liu, Y. Liu, S. Xu, Y. Ha, Y. Guo, X. Yu, D. Sun and F. Fang, *J. Mater. Chem.A*, 2018, **6**, 10304-10312.
28. Z. Chen, Y. Ha, Y. Liu, H. Wang, H. Yang, H. Xu, Y. Li and R. Wu, *ACS Appl Mater Interfaces*, 2018, **10**, 7134-7144.
29. J. Zhao, X. Li, G. Cui and X. Sun, *Chem. Commun.*, 2018, **54**, 5462-5465.
30. M. Xie, X. Xiong, L. Yang, X. Shi, A. M. Asiri and X. Sun, *Chem. Commun. (Camb.)*, 2018, **54**, 2300-2303.
31. X. Xiao, C.T. He, S. Zhao, J. Li, W. Lin, Z. Yuan, Q. Zhang, S. Wang, L. Dai and D. Yu, *Energy Environ. Sci.*, 2017, **10**, 893-899.
32. X. Xiong, Y. Ji, M. Xie, C. You, L. Yang, Z. Liu, A. M. Asiri and X. Sun, *Electrochem. Commun.*, 2018, **86**, 161-165.
33. L. Hui, Y. Xue, D. Jia, H. Yu, C. Zhang and Y. Li, *Adv. Energy Mater.*, 2018, 1800175.
34. C. Tang, R. Zhang, W. Lu, L. He, X. Jiang, A. M. Asiri and X. Sun, *Adv.Mater.*, 2017, **29**, 1602441-n/a.
35. P. W. Menezes, A. Indra, C. Das, C. Walter, C. Göbel, V. Gutkin, D. Schmeiβer and M. Driess, *ACS Catalysis*, 2016, **7**, 103-109.
36. G. Read, J. F. Callejas, C. F. Holder and R. E. Schaak, ACS Appl Mater Interfaces, 2016, **8**, 12798-12803.
37. T. Wang, L. Wu, X. Xu, Y. Sun, Y. Wang, W. Zhong and Y. Du, Sci. Rep., 2017, **7**, 11891.

38. J. Hou, Y. Sun, Z. Li, B. Zhang, S. Cao, Y. Wu, Z. Gao and L. Sun, *Adv. Funct. Mater.*, 2018, **28**, 1803278.
39. P.Z. Chen, M.X. Zhang, Y. Tong, C.G. Zhong, N. Zhang, and L.D. Zhang, and Y. Xie, *Adv. Mater.*, 2017, **29**, 1701584.
40. Y.Q Sun, Z.X. Wei, H.L. Li, T. Zhang, X.Y. Li, W.P. Cai, and J.M. Ma, *Adv. Mater.*, 2018, 1802121.
41. A.P. Wu, Y. Xie, H. Ma, C.G. Tiana, Y. Gua, H.J. Yan, X.M. Zhang, and G.Y. Yang. *Nano Energy.*, 2018, **44**. 353–363.
42. C. P. Prashanth, W. Menezes, S. Garai, C. Walter, A. Guiet, and a. M. Driess, *Angew. Chem.*, 2018, **130**, 15457 –15462.
43. L. L. Zheng, S.G. Mo, D.H. Ou, J. Tao, R.X. Qin, and X.L. Fang, *Small.*, 2018, **14**, 1800759.
44. Y.M. Xin, L.Y. Gan, and Z.H. Zhang, *ACS Nano.*, 2017, **11**, 10303-10312.
45. J. W.Jin, D.F. Su, Z.Z.e Wei, Z.F. Pang, and Y. Wang, *J. A. Chem. Soc.*, 2015, **137**, 2688-2694.
46. Y.Y. Chen, S.F. Jin, and F. Gao, *J. A. Chem. Soc.*, 2017, **139**, 8320-8328.
47. K. Y. Pan, S.J. Liu, X. Cao, K.L. Wu, W.C. Cheong, and Y. Li, *J. A. Chem. Soc.*, 2018, **140**, 2610-2618.
48. X. W. Han, Y. Deng, J. Liu, J. Lu, C. Zhong, and W. Hu, *Adv. Energy Mater.*, 2018, **8**, 1800935.
49. M. Z. Yu, Y. Tong, C. Li, and G.Q. Shi, *Adv. Energy Mater.*, 2018, 1800403.
50. Y. D. Yu, M.R. Gao, C.C. Lang, Y.R. Zheng and S.H. Yu, *Chem. Sci*, 2017, **8**, 968–973.